RSC Advances

Evaluation of three dimensional high nitrogen doped graphene as an efficient sorbent for the preconcentration of BTEX compounds in environmental samples

Journal:	*RSC Advances*
Manuscript ID	RA-ART-10-2015-021397.R1
Article Type:	Paper
Date Submitted by the Author:	07-Dec-2015
Complete List of Authors:	Tabani, Hadi; Shahid Beheshti university, chemistry Khodaei, Kamal; Research Institute of Applied Sciences (ACECR) Kazemi Movahed , Siyavash ; Shahid Beheshti University Zeraatkar Moghaddam , Ali ; University of Birjand Dorabadi Zare , Farzaneh ; Shahid Beheshti University Mirzaei , Saeed ; Research Institute of Applied Sciences (ACECR)
Subject area & keyword:	Separation science < Analytical

Evaluation of three dimensional high nitrogen doped graphene as an efficient sorbent for the preconcentration of BTEX compounds in environmental samples

Hadi Tabani *[,a], Kamal Khodaei [a], Siyavash Kazemi Movahed [b], Ali Zeraatkar Moghaddam [c], Farzaneh Dorabadi Zare [b], Saeed Mirzaei [a]

[a] *Department of Environmental Geology, Research Institute of Applied Sciences (ACECR), Shahid Beheshti University, Tehran, Iran*

[b] *Department of Pure Chemistry, Faculty of Chemistry, Shahid Beheshti University, G. C., P.O. Box 19396-4716, Evin, Tehran, Iran*

[c] *Department of Chemistry, Faculty of Sciences, University of Birjand, Birjand, Iran*

* Corresponding author: Dr. Hadi Tabani, Department of Environmental Geology, Research Institute of Applied Sciences (ACECR), Shahid Beheshti University, Tehran, Iran.

Tel & Fax: +98 (21) 22431661

E-mail: hadi_tabani@yahoo.com (H. Tabani)

Abstract

Introducing a new class of sorbents is an interesting work and this issue is a hot topic in the field of sample preparation. In this study, for the first time, three dimensional high nitrogen doped graphene (3D-HND-G) was synthesized as a new sorbent and then it was successfully applied for the quantification of BTEX compounds in environmental samples using gas chromatography. Firstly, the extraction efficiency of various carbon nanostructures including graphene (G), graphene oxide (GO), nitrogen doped graphene (ND-G), high nitrogen doped graphene (HND-G), and 3D-HND-G were compared. The results revealed that 3D-HND-G had higher efficiency for the extraction of BTEX compounds. Better dispersibility and higher surface area of 3D-HND-G rather than other carbon nanostructures may be the main reason of this phenomenon. Box–Behnken design methodology and the response surface methodology were applied to find out the optimal experimental conditions. The Optimized extraction conditions were: sorbent amount, 70 mg; sorption time, 8 min; salt concentration, 6.5% w/v; type and volume of the eluent, 255 µL methanol. Under the optimized conditions, the enrichment factors were obtained within the range of 328–376, which corresponds to extraction recoveries of 82–94%. The limit of detection and quantification were in the range of 0.5-1 ng mL^{-1} and 1.5-3 ng mL^{-1}, respectively. The method was reproducible since the intra and inter day precision (RSDs%, n = 5) were less than 6.2%. Finally, the proposed method was successfully applied to determine the concentration of BTEX as hazardous materials in the environmental samples.

***Keywords*:** Carbon nanostructures; Environmental samples; Experimental design; Gas chromatography; Nitrogen doped graphene.

Introduction

Volatile organic hydrocarbons (VOHs) are organic chemical compounds that have high enough vapor pressures under normal conditions to significantly vaporize and enter the atmosphere. BTEX that stands for benzene, toluene, ethyl benzene, and xylene are among the VOHs found in petroleum products, such as gasoline and diesel fuel, and also various organic chemical formulations of products. Beside their useful applications in human life, negative effects of BTEX must be discussed. These compounds are known as pollutants and are typically found near petroleum production and storage sites.[1-3] BTEX compounds frequently enter soil, sediment and groundwater due to accidental oil spill, leakage of gasoline and other petroleum fuels from underground storage tanks and pipelines, and improper oil-related waste disposal practices and therefore they seriously affect human health.[4] Also, BTEX can be absorbed by human body through skin or respiratory system.[5] For example, short exposure of benzene on human body leads to drowsiness, headaches and dizziness, however long exposure can be a reason of leukemia.[6] Toluene, ethylbenzene and xylenes negatively affect the central nervous system, disturb coordination, cause drowsiness, headache and mental disorders.[7,8] Environmental Protection Agency (EPA) set the maximum contaminant level (MCL) for benzene, toluene, ethyl benzene, and xylenes in drinking water at 5, 1000, 700, and 10000 $\mu g\ L^{-1}$, respectively.[9] Therefore, the presence of these compounds in water sources is highly objectionable for human and animal consumption. Due to the fact that the major sources of drinking water are groundwater and river water, monitoring the BTEX compounds in these water sources is quite necessary.

Despite all the innovations and improvements of selective and sensitive analytical instruments, sample preparation is often an indispensable and crucial step for the determination of analytes at

trace levels in complex matrices, especially environmental and biological samples. A serious problem encountered in the determination of BTEXs is that they usually present in water at very low concentrations, resulting in poor analytical accuracy and precision. Therefore, it is of vital importance to develop sensitive and reliable extraction and preconcentration approaches for BTEXs prior to their instrumental determination.

A diverse array of sample preparation methods including liquid–liquid extraction (LLE),[10] solid phase extraction (SPE),[11] solid phase microextraction (SPME),[12-15] single drop microextraction (SDME),[16,17] dispersive liquid–liquid microextraction (DLLME),[18-20] and hollow fiber liquid phase microextraction (HF-LPME)[21,22] have been widely used for the extraction of BTEX compounds in environmental samples.

SPE is a widely used technique for environmental sample pretreatment due to its high recovery, short extraction time, high enrichment factor, and ease of automation. The choice of an appropriate sorbent is a critical fact to obtain good recovery and high enrichment factor in SPE procedure. Recently, numerous carbon nanomaterials including carbon nanotubes (CNTs),[23] carbon nanohorn,[24] nanoparticle of microgel,[25] and carbon nanocones/disks[26] have been widely used as adsorbents in SPE techniques due to their large specific surface areas, high adsorption capacity and good chemical and thermal stability.

Graphene (G), a new class of carbon nanomaterials, has recently sparked much interest due to its unique strict two-dimensional nanostructure which makes it a superior candidate as an adsorbent for SPE and SPME.[27-30]

Recently, three-dimensional graphene (3D–G) nanostructures were directly synthesized by chemical vapor deposition (CVD), which comprised network and porous structures that may offer higher surface area, electrical conductivity, and good mechanical properties.[31] But, the

main drawback of G nanostructures is the low dispersibility of these materials in aqueous media. For this reason, in this study, G nanostructures were doped with various amounts of nitrogen (N). In general, chemical doping with N is considered as an effective method to intrinsically modify the properties of carbon materials. Nitrogen doping plays a critical role in regulating the chemical properties of carbon materials due to their comparable atomic size and its five valence electrons available to form strong valence bonds with carbon atoms. Theoretical study has shown that nitrogen doping results in a higher positive charge on a carbon atom adjacent to the nitrogen atoms,[32] and a positive shift of Fermi energy at the apex of the Brillouin zone of G.[33] Also, the introduction of N groups into G nanoparticles improves the dispersibility of these materials in water and the electrostatic repulsion caused by N group prevents any aggregation.[34]

Therefore, in this study, we focused on introducing three dimensional high nitrogen doped graphene (3D-HND-G) as a new sorbent for SPE procedures. For this purpose, N- doped G nanoparticles were synthesized with different percentages of N and were used for the extraction and determination of BTEX in environmental samples. To the best of our knowledge, it is the first report on employing a 3D-HND-G as sorbent. Box-Behnken design (BBD) was used to optimize the influence of different experimental conditions in the extraction procedure. Finally, the optimized procedure was employed to determine these contaminants in five river water samples as environmental samples.

Experimental

Reagents and materials

Benzene (99.8% purity), toluene (99.9% purity), ethyl benzene (99.8% purity), and o-xylene (97% purity) were purchased from Sigma–Aldrich (St. Louis, MO, USA). All the analytical grade solvents including methanol, acetone, acetonitrile, propane, cyclohexane, and 1-octanol

were purchased from Merck (Darmstadt, Germany). $KMnO_4$, $K_2S_2O_8$, P_2O_5, H_2O_2, H_2SO_4, HCl, Urea, hydrazine hydrate, Ammonia, and ethylene diamine (EDA) were purchased from Fluka (Buchs, Switzerland). The G and GO were purchased from Research Institute of the Petroleum Industry (Tehran, Iran). HPLC grade water was obtained through a Milli-Q® system (Millipore, Milford, MA, USA) and was used to prepare all solutions.

Apparatus

The Fourier transform infrared (FT-IR) measurements were carried out using a Bomem MB-Series FT-IR spectrometer in the form of KBr pellets. The X-ray diffraction (XRD) patterns were collected on STOE STADI P with scintillation detector, secondary monochromator and Cu-Ka1 radiation (λ =1. 5406 Å). X-ray photoelectron spectroscopy (XPS) analysis was performed using a Gammadata-scienta ESCA 200 hemispherical analyzer equipped with an Al Ka (1486.6 eV) X-ray source. Raman spectra of nanostructures were recorded on a Bruker SENTERR (2009) with an excitation beam wavelength at 785 nm. Scanning electron microscope (SEM) image of 3D-HND-G was obtained on a Hitachi S-4160 SEM. Transmission electron microscope (TEM) images of ND-G, HND-G, and 3D-HND-G nanostructures were taken using Philips CM-30 transmission electron microscope with an accelerating voltage of 150 kV and Zeiss EM10C transmission electron microscope with an accelerating voltage of 80 kV. The CHNS analysis was performed on a Thermo Finnigan Flash EA112 elemental analyzer (Okehampton, UK). Ultrasonic bath (Eurosonic 4D ultrasonic cleaner with a frequency of 50 kHz and an output power of 350 W) was used to disperse materials in aqueous samples.

Separation, identification and quantification were carried out on a gas chromatograph (GC) model GC-15A from Shimadzu Company (Tokyo, Japan) equipped with a split / splitless capillary injection port and a flame ionization detector (FID). A CP-Sil-8 fused silica capillary

column (25 m × 0.32 mm i.d. and 0.52 µm film thickness) from Chrompack was employed. Samples were injected in splitless mode and nitrogen was used as the carrier gas at the constant flow rate of 2.0 mL min^{-1}. The temperatures of the injector port and the detector were 220 and 280°C, respectively. The column oven was initially held at 50°C for 3 min, programmed to 120°C by ramp of 10°C min^{-1} and then raised to 260°C by ramp of 15°C min^{-1}. A Lab-solutions program was used for acquiring and processing the data.

Standard, reference material **and real environmental sample solutions**

A stock solution containing 1000 mg L^{-1} of each BTEX compounds was prepared in methanol. The stock solution was protected from light exposure using aluminum foil and stored at 4 °C. Then, the required working standard solutions were freshly prepared by diluting an appropriate amount of the stock solutions with HPLC grade water.

The certified reference material (CRM), TraceCERT®, 200 µg mL^{-1} of each BTEX compound in methanol as ampule of 1.0 mL, was purchased from Sigma–Aldrich (St. Louis, MO, USA). Then for investigation of trueness of the proposed method, this CRM was diluted with HPLC grade water for preparation of 30 and 100 ng ml^{-1} of each BTEX compound.

Five river water samples were collected from Kan, Jajrood, Farahzad, Talab Bande Alikhani, and Mohammadieh in Tehran, Iran to serve as real environmental samples. These real samples were collected in clean polyethylene bottles after filtering through a 0.45 µm membrane filter (MSI, Westboro, MA, USA) and were kept at 4 °C.

Preparation of ND-G

The pH of the aqueous dispersion of GO (70 mL, 140 mg) was adjusted at 10 using ammonia 30%. Then, 2 mL of hydrazine hydrate was added while stirring magnetically for 10 min. The solution was then transferred into a Teflon-lined autoclave and heated at 80 ºC for 3 h. The

reduced G sheets were collected with centrifugation, followed by washing several times with deionized water and were then dried in vacuum oven at 50 °C.[35,36]

Preparation of HND-G

An aqueous dispersion solution of GO (10 mL, 40 mg) was diluted with 25 mL of deionized water, and then urea (12 g) was added into the GO dispersion under sonication for 3 h. After that, the solution was sealed in a 50 mL Teflon-lined autoclave and maintained at 180 ºC for 12 h. The solids (N-doped graphene sheets) were filtered and washed several times with distilled water. Finally, the sample was collected and dried in a vacuum oven at 80 ºC.[35, 37]

Preparation of 3D-HND-G

GO dispersion (90 mg, 30 mL) was mixed uniformly with 120 μL of EDA by sonication for 5 min. The resulting stable suspension was transferred into a 50 mL Teflon-lined autoclave and heated for 6 h at 120 °C for the synthesis of the 3D-G hydrogel.[35, 38] After subsequent freeze-drying, the 3D-HND-G aerogel was produced.

Extraction procedure

Batch experiments were used for the investigation of factors in extraction steps. Extracting the BTEX from standard solutions and real samples is accomplished through two steps: sorption and desorption. In the sorption step, 70 mg of G nanoparticle was suspended in 100 mL of an aqueous solution containing 100 ng mL^{-1} of each BTEX compounds and the solution was stirred at a constant rate of 1250 rpm to facilitate mass transfer and sorption of the model analytes onto the sorbent. After extracting the solution for a prescribed period of time (8 min), G nanoparticles were separated from the solution by filtration. In the desorption step the sorbent was transferred to a conical tube and then it was eluted with 255 μl methanol by fierce vortex for 1.0 min.

Finally, the eluate was isolated from the sorbent by the centrifuge and 1.0 µl of the eluent was withdrawn into a microsyringe and then injected into the GC-FID for further analysis.

Data analysis and statistical methods

In order to obtain optimal conditions and investigate the interaction of variables, a BBD was employed. The experimental design matrix and data analysis were performed by the Statgraphics Plus Package (version 5.1; Statistical Graphics, Manugistics, USA).[39]

Results and discussion

Characterization of the nanosorbents

Raman spectroscopy is a very useful tool for investigating the electronic and phonon structure of the graphene-based materials.[40] The Raman spectra of prepared GO, ND-G, HND-G and 3D-HND-G are shown in Figure 1. The characteristic D and G bands of carbon materials are observed at around 1285 and 1570 cm^{-1}, respectively. The D band is characteristic of a breathing mode for k-point phonons of A_1g, while the G band is the result of the first-order scattering of the E_{2g} mode of sp^2 carbon domains.[41] Both bands can be influenced by doping.[42] The D bands are significantly enhanced in ND-G and HND-G in comparison with GO since pyridinic and pyrrolic nitrogens are accompanied by defects inside the G network and by the functional edges of G sheets (Figure 2). The G bands of ND-G, HND-G and 3D-HND-G shift to the higher frequencies (9.94, 8.77, 28.88 cm^{-1} respectively) with respect to that of GO. Previous theoretical simulations on N-doped carbon nanotubes suggested that substitution of carbon atoms with graphitic nitrogens was n-type doping, while for pyridinic and pyrrolic nitrogens was p-type doping. Since ND-G, HND-G and 3D-HND-G contain more pyridinic and pyrrolic nitrogens, G band shifts in these materials are in agreement with the earlier observation of upshift in p-type doped graphite and carbon nanotubes. The intensity ratio of G-band and D-band (I_D/I_G) is a general parameter, reflecting the carbon hybridization state of materials and the degree of disorder.[43] As shown in Figure 1, after the introduction of N on GO sheets, the I_D/I_G were 1.57, 1.58 and 1.95 for the resulting ND-G, HND-G and 3D-HND-G, respectively, while the I_D/I_G of GO was 1.49. The higher value of I_D/I_G observed for ND-G, HND-G and 3D-HND-G clearly demonstrate the heteroatomic doping of N into the G frame and the enhanced degree of disorder.[44]

Figure (3a-c) shows a comparison between the morphologies of ND-G, HND-G, and 3D-HND-G, investigated by TEM. The micrograph of ND-G and HND-G possess similar wrinkled sheet morphology (Figure 3a, b).

The 3D morphology of as-prepared 3D-HND-G was confirmed by SEM characterization (Figure 3d). The 3D-HND-G exhibits a foam-like structure with interconnected pores ranging from tens to hundreds of micrometers. Additionally, TEM observation revealed the developed graphitic structure in these folded and crumpled regions (Figure 3c) which may contribute to enhancing their mechanical properties.[44]

The XRD patterns of the original GO, ND-G, HND-G and 3D-HND-G were displayed in Fig. 4. The diffraction peak located at $2\theta = 10.1°$ is attributed to the (002) crystalline plane of GO and the corresponding calculated interlayer spacing is about 0.79 nm. However, the peak at $2\theta= 10.1°$ entirely disappeared after hydrothermal reaction, and a broad diffraction peak around 25° of the graphite (002) plane was observed for the synthesized ND-G, HND-G and 3D-HND-G sample, indicating the framework of the reduced sample was composed of few-layer stacked G nanosheets.[37]

FT-IR spectra of ND-G, HND-G and 3D-HND-G are shown in Fig. 5. The peak intensity of carbonyl (C=O) at 1722 cm^{-1} of the 3D-HND-G obviously decreases, compared with that of GO. Moreover, the peak of epoxy C–O–C at 1226 cm^{-1} almost disappears in 3D-HNG, which implies the efficient reduction of GO and subsequent assembly of G sheets into 3D structures.[45] A new peak is certainly identified at about 1550 cm^{-1} which can be assigned to sp^2 bonded C=N, demonstrating the formation of the C–N bond in the formation of 3D-HND-G, HND-G and ND-G.[46]

XPS is an effective tool to identify the states of elements, and to study the nitrogen–doping effect in G.[37] As shown in Fig. 6, the peaks corresponding to C 1s, N 1s and O 1s, were clearly observed in the XPS survey spectra. From the N 1s XPS scan shown in Fig. 6, it is observed that three different types of nitrogen are present in the ND-G, HND-G and 3D-HND-G systems. As can be seen, *N*-pyridinic (N^1, 398 eV) contributes to the π-conjugated system with a p-electron in the G layers; *N*-pyrrolic (N^2, 399 eV) refers to the *N* atom contributing two p-electrons to the π system, which is ascribed to the contribution of pyridine and pyrrol functionalities, respectively; *N*-quaternary (N^3, 401 eV) is derived from the *N* atoms that replace the C atoms in grapheme hexagonal-ring.[37]

In order to confirm the synthesis of these carbon nanostructures and also compare the amounts of N present in their structures, the atomic percentage of carbon, hydrogen, and nitrogen was monitored using CHNS analysis. The weight percentage of N, C, H and N/C ratio of composites are shown in Table 1. As shown in this Table, the atomic percent of N is 3.19%, 11.24%, and 17.44% for ND-G, HND-G, and 3D-HND-G, respectively which confirms the successful synthesis of mentioned nanostructures.

Optimization strategy

To obtain the maximum extraction recoveries for simultaneous extraction of BTEX compounds, the effective parameters of SPE including, type of the sorbent, type of the eluent solvent, the pH of the sample solution, extraction time, amount of the sorbent, ionic strength, and volume of the eluent were optimized. Initially, the influence of pH of the sample solution, type of the sorbent and eluent on extraction efficiency was evaluated using one variable at a time (OVAT) methodology. Then, the influence of the other factors (extraction time, amount of sorbent, ionic

strength, and volume of the eluent), was evaluated by BBD methodology. The levels of the factors were selected based on preliminary experiments and they are shown in Table 2.

Sorbent type

The sorbent type is a crucial variable affecting the extraction efficiency. In this context, extraction abilities of G, GO, ND-G, HND-G and 3D-HND-G, were investigated comprehensively (Fig. 7). Whereas, π-π interaction is a main driving force for the sorption of all analytes on carbon skeleton thus better dispersibility of sorbent would improve this kind of interaction. The results revealed that ND-G, HND-G, and 3D-HND-G can act as the best sorbents due to the presence of N groups and higher dispersibility of these sorbents compared to that of G and GO. The introduction of N groups into G nanoparticles improved the dispersibility of these materials in aqueous media and the electrostatic repulsion by N group prevented further aggregation. Thus, 3D-HND-G with a higher amount of nitrogen (17%) and a network structure could lead to an increased surface area available for adsorption. This issue and also its better dispersion in aqueous media may result in better extraction efficiency. This result can be conclude through the comparison of extraction efficiencies between HND-G with ND-G, so that HND-G which has 12% N in its structure showed higher extraction efficiency in comparison with ND-G with 4% N.

Also, better extraction efficiency of GO in comparison with G can be attributed to the fact that GO contains a number of oxygen-containing polar functional groups, such as –COOH and –OH, so the polarity and dispersibility of it is higher than that of G. Thus, 3D-HND-G was selected as the most appropriate sorbent for the rest of the studies.

Selection of the desorption solvent

After sorption, the analytes should be eluted from the sorbent using an appropriate eluent solvent prior to GC analysis. The elution of the target analytes was explored using different organic solvents, i.e. methanol, acetone, acetonitrile, propane, cyclohexane, and 1-octanol. Other factors were kept constant during the optimization (extraction time, 10 min; 50 mg of 3D-HND-G; elution volume, 500 μL). The results showed that the desorption ability of methanol was higher than the other solvents. This can be explained by suitable solubility of the BTEX compounds in methanol. Hence, methanol was chosen as the best elution solvent.

Influence of the pH of the sample

The pH of the sample was investigated between 2.0 and 10.0 to determine the optimum pH of the sample. Figure 8 showed that the change of pH in the range of 2.0 to 8.0 had no significant effect on the extraction efficiency. The changes in solution pH during BTEX adsorption on 3D-HND-G sorbent were insignificant implying that BTEX were in the molecular forms during adsorption process. Although, at higher pH than 8.0 the extraction efficiency was gradually decreased. This can be attribute that in these pHs the pyridinic and pyrrolic nitrogens of 3D-HND-G were deprotonated and this sorbent was in the neutral's form. Thus, the dispersibility of the 3D-HND-G in the aqueous media was decreased. Considering the pH value of the aqueous sample containing BTEX is close to 7, the pH in water sample was kept as its initial value without deliberately adjustment in the following experiments.

Optimization design

The BTEX compounds were extracted from 100 mL of sample solutions. First, the extraction conditions were optimized for water, and then the conditions were applied to environmental samples. Different variables which can affect the extraction efficiency were optimized by a BBD methodology. BBD does not contain any points at the vertices of the cubic region created by the

upper and lower limits for each variable; which means the reduced number of required runs. This could be advantageous when the points on the corners of the cube represent factor-level combinations that are prohibitively expensive or impossible to test because of physical process constraints. This design is suitable for exploring quadratic response surface and constructing second-order polynominal models. Experimental data were fitted to a quadratic polynomial model and regression coefficients were obtained. The non-linear computer-generated quadratic model used in the response surface was as follows:

$$Y(x) = \beta_0 + \sum_{i=1}^{4} \beta_i X_i + \sum_{i=1}^{4} \beta_i X_i^2 + \sum_{i=1}^{4}\sum_{j=1}^{4} \beta_{ij} X_i X_j \quad (1)$$

where, Y(x) is the response , β_o is an intercept, β_i and β_{ij} are constant regression coefficients of the model, and X_i, X_j (i = 1,4; j = 1,4 and i≠j) represent the coded level of an independent variable. Thus, in this step, a BBD was applied for the modeling of four factors (extraction time, amount of the sorbent, ionic strength, and volume of the eluent) and investigating the interaction among these variables.

The total number of experiments (N) was calculated as follows:

$$N = 2k\,(k-1) + Cp \quad (2)$$

where k is the number of variables and C_p is the number of centre points.[47] Thus, experimental design consists of 30 experiments with six center points (in order to allow the estimation of pure error) and it allows the calculation of the response function at intermediate levels and enables the estimation of the system performance at any experimental point within the studied range. Normalized peak area was used as the experimental response for each run. Normalized peak area was average peak areas of BTEX compounds.

One of the important parameters for evaluating the model is adjusted R-squared (R^2_{adj}). This parameter can be considered as a measure of the amount of variation around the mean explained

by the model adjusted for the number of terms in the model. In addition, predicted R-square (R^2_{pred}) which is a measure of the amount of variation in new data explained by the model can be applied for the evaluation of the model. The R^2_{pred} and the R^2_{adj} values should be within 0.20 of each other, otherwise there may be a problem with either the data or the model. The R^2_{pred} and the R^2_{adj} values for the above model were 0.97 and 0.95, respectively.

Also, this result can be interpreted with analysis of variance (ANOVA) by F-ratio and P-value which are presented in Table 3. If the P-value of a factor or interaction between factors is higher than 0.05, it means that it does not have a dominant effect, while a factor with P-value lower than 0.05 would be significant. In order to estimate the adequacy of the proposed equation, the residual sum of squares has been split into two parts consisting of pure experimental error and inadequacy of model (lack of fit). The lack of fit test is designed to determine whether the selected model is adequate to describe the observed data, or whether a more complicated model should be used. The test is performed by comparing the variability of the current model residuals to the variability between observations at replicate settings of the factors. Since the P-value for lack of fit in the ANOVA table is higher than 0.05, the model appears to be adequate for the observed data at the 95.0% confidence level.

The ANOVA results produced the Pareto chart of main and interaction effects which are shown in Fig. 9. In this chart, the bar lengths are proportional to the absolute value of the estimated main effects. Fig. 9 also includes a vertical line corresponding to the 95% confidence interval. An effect, which exceeds this reference line, may be considered significant as regards the response. A positive value for the estimated effect indicates an increase in the response if the variable increases to its high level. A negative value indicates that a better response is obtained at low levels of the variable. For the interactions, a positive value indicates that the response will

increase if both variables change to the same level, low or high. A negative value indicates an increase in the response if the variables change in opposite directions (one variable increases to a high level and the other decreases to a low level). According to the Pareto chart, four factors and the interaction between some of them showed statistically significant effects at the $p < 0.05$ level. Also, this figure shows that volume of eluent has a negative effect upon the extraction while the other factors show a positive effect upon the extraction efficiency.

The response surface methodology (RSM) and two dimensional (2D) contour plot (Fig. 10A) were applied to analyze simultaneous effects of the extraction time and amount of the sorbent on the response plot that revealed the interaction between these independent variables. The sorption efficiency of analytes increased along with the increase in extraction time and amount of the sorbent. Moreover, the extraction time and the sorbent amount both showed positive effect on the extraction efficiency and were the second and third important factors, respectively.

Also, the RSM and 2D contour plot were applied to analyze simultaneous effect of salt content and volume of the eluent on the response and displayed the interaction between these independent variables (Fig. 10B). Salt addition generally promotes the extraction efficiencies of polar analytes due to the salting-out effect. For non-polar analytes, this effect is generally not significant. Based on this figure, the normalized peak area initially increased with the increase of NaCl concentration up to 6.5%, followed by a descent with further increase of NaCl concentration. This result can be explained by the two simultaneously existing opposite processes: the salting out effect and the electrostatic interactions between compounds and the salt ions in the sample solution. At first, the former process was predominant that the extraction efficiency increased with the increase of NaCl concentration. However, with the further increase of NaCl concentration, the target compounds participated in electrostatic interaction with salt

ions in the solution,[48] which directly decreased the normalized peak area. The eluent volume affects the sensitivity of the method, as it determines the maximum preconcentration factor that can be achieved for the target analytes. The experimental results indicated that 255 μL of eluent is sufficient to obtain satisfactory recoveries and acceptable preconcentration factors for the BTEX compounds. As can be seen in Fig. 10B, for eluent volumes more than 255 μL, normalized peak area decreased due to the dilution effect.

According to the overall results of the optimization study, the following experimental conditions were chosen: extraction time, 8 min; 255 μL methanol as the eluent solvent; 70 mg of 3D-HND-G as sorbent; and 6.5% (w/w) NaCl.

Adsorption isotherms

Adsorption isotherms are a basic requirement in understanding how the adsorbate is distributed between the liquid and solid phases when the adsorption process reaches an equilibrium state.[49] Distribution of analytes between the liquid phase and the solid phase can be described by several isotherm models such as Langmuir and Freundlich.

The Langmuir isotherm assumes monolayer adsorption onto a surface containing a finite number of adsorption sites of uniform strategies with no transmigration of adsorbate in the plane surface.[50] Once a site is filled, no further sorption can take place at that site. This indicates that the surface reaches a saturation point where the maximum adsorption of the surface will be achieved. Its linearized form can be represented as:[51]

$$\frac{C_e}{Q_e} = \frac{1}{K_l \,.\, Q_m} + \frac{C_e}{Q_m} \qquad (3)$$

where C_e is the concentration of analyte in solution at equilibrium (mg L^{-1}), Q_m is the monolayer capacity of the sorbent (mg g^{-1}) and, K_l is the Langmuir constant (L mg^{-1}) that is relevant to the free energy of adsorption stage. The sorption capacity (Q_e) described as the maximum amount of

analytes sorbed per gram of the adsorbent is an important factor for the evaluation of the synthesized sorbent and it was calculated using the following equation:

$$Q_e = (C_o - C_t) \times V/M \quad (4)$$

where C_o is the initial concentration, C_t is the concentration at any time, V is the sample volume and M is the weight of the adsorbent (g).

The Freundlich model is an empirical expression that assumes a heterogeneous adsorbent surface with sites that have different energies of adsorption and are not equally available. The Freundlich isotherm model is usually explained for multilayer adsorption on a heterogeneous adsorbent surface and is given in the form of a linearized equation:[52]

$$Log\ Q_e = Log\ K_f + \frac{1}{n}\ LogC_e \quad (5)$$

where K_f and n are Freundlich constants which correspond to adsorption capacity and adsorption intensity, respectively.

The equilibrium adsorption isotherm was obtained by utilizing batch studies. Briefly, 100 mL of the sample solution (pH = 7.0) with different initial BTEX concentrations (10–50 mg L^{-1}), and 200 mg of 3D-HND-G were placed in test vial. Then, the adsorption step was done under optimal condition.

The values of the Langmuir and Freundlich isotherm constants were calculated from the slope and intercept of the plots of C_e/Q_e versus C_e (Figure 11) and Log Q_e versus Log C_e (Figure 12), respectively; the results are shown in Table 4. The Freundlich model gave a better fitting of the sorption data than the Langmuir model, as is evident from the higher R^2 values. This suggests that the adsorption of BTEX on 3D-HND-G occurs through multilayers (heterogeneous surface).

The n value indicates the degree of nonlinearity between solution concentration and adsorption as follows: if $n = 1$, then adsorption is linear; if $n < 1$, then adsorption is a chemical process; if n

> 1, then adsorption is a physical process and indicates favorable adsorption.[53] In the present study, since n are in the range of 1.23-1.29 (Table 4), it indicates the physical adsorption of BTEX on 3D-HND-G.

Validation of the method

Quality features of the current method were evaluated under the final opted conditions to assess the method performance. Some analytical features such as limit of detection (LOD), limit of quantification (LOQ), linearity, correlation coefficients (r), precision, and recovery (R) are shown in Table 5. The LOD for each compound in water sample was determined at a concentration where the signal to noise ratio was equal to 3. The LOD values were obtained within the range of 0.5–1 ng mL^{-1} and were below the maximum allowable amount for drinking water. The intra-day precision (repeatability) of the proposed method, expressed as RSD%, was evaluated by extracting five independent samples spiked at 60 ng mL^{-1} with each analyte and it was found to be in the range of 4.2–5.0%. The inter-day precision was investigated by analyzing samples spiked at 60 ng mL^{-1} with each analyte for five consecutive days and the RSD% values were found to be in the range of 4.5–5.2% (Table 5).

The recovery (R) was defined as the percentage of the number of moles of the analyte adsorbed onto the sorbent (n_f) to those originally present in the sample solution (n_i).

$$R\% = \frac{n_f}{n_i} \times 100 \quad (6)$$

Relative recovery (RR) was acquired from the following equation:

$$RR\% = \frac{C_{found} - C_{real}}{C_{added}} \times 100 \quad (7)$$

where C_{found}, C_{real}, and C_{added} are the concentration of analyte after the addition of a known amount of the standard into the real sample, the concentration of analyte in real sample, and the

concentration of a known amount of standard which was spiked into the real sample, respectively. Good recoveries were found in the range of 82-94 % (Table 5).

Certified reference material and real sample analysis

To confirm that the method is suitable for its intended use, a validation process was carried out by establishing the basic analytical requirement of the performance quantification of BTEX in CRMs (Table 6). The concentrations obtained for the BTEX compounds showed an acceptable agreement with the certified results and the high relative recoveries (98.3-100.5%) indicated this issue.

In order to check the potential matrix effects and investigate the applicability of the method in real sample analysis, five river water samples (Kan, Jajrood, Farahzad, Talab Bande Alikhani, and Mohammadieh) were tested (Table 7). The results indicated that Kan, Jajrood, and Mohammadieh were free of BTEX compounds or their concentrations were below detection limits of the proposed method. But in Talab Bande Alikhani sample, 68 and 45 ng mL^{-1} of benzene and toluene, and in Farahzad sample 24 and 32 ng mL^{-1} of benzene and toluene were determined, respectively. The presence of these compounds was confirmed by spiking a standard solution (60 ng mL^{-1}) of each BTEX compound into these samples and reanalyzing them. All nonspiked and spiked chromatograms of these real samples are depicted in Fig. 13. For instance, as shown in the spiked chromatogram for Talab Bande Alikhani sample, the benzene and toluene peaks are higher than ethyl benzene and o-xylene at the same spike concentration (60 ng mL^{-1} of each BTEX compound) (Figure 13B). That means, benzene and toluene exist in this river water sample (non-spiked).

To investigate the matrix effects, these environmental samples were spiked with BTEX compounds at 60 ng mL^{-1} level and their relative recoveries were determined to be in the range

of 93–104% (Table 7). These high relative recoveries indicated a negligible matrix effect on SPE efficiency in these samples.

A comparison between the proposed method with other methods applied for the extraction of BTEX compounds is summarized in Table 8. The results showed an excellent applicability of the method for the determination of these compounds in environmental samples. One can see that along with simple equipment, the proposed method offers excellent enrichment factors and LODs in a relatively short time. Therefore, coupling GC-FID with the proposed method can provide good and sensitive results for the determination of these compounds in environmental samples.

Conclusions

In this study, for the first time, we demonstrated the application of 3D-HND-G nanoparticle as a new sorbent for extraction of BTEX as model compounds. Comparing the results between carbon nanostructures (G, GO, ND-G, HND-G, and 3D-HND-G) showed that there are two main factors for improving the extraction efficiency. One of them is the structure and surface area of the sorbent, and another one is the percentage of N in the structure of the sorbent. Thus, combining the advantages of a well-defined 3D structure and doped nitrogen atoms, the obtained free-standing 3D-HND-G exhibited high efficiency for the extraction of BTEX compounds. The 3D structure with higher surface area and higher percentage of N not only can increase the adsorption ability of the target analytes, but also improves the dispersibility of these nanocarbons in aqueous media. The accuracy of the method was verified by analyzing CRM and proved to be satisfactory. Considering short extraction time, as well as satisfactory LOQ and RSD, good enrichment factor, and also the capability of extraction with low volume of an organic solvent,

3D-HND-G sorbent may have a strong potential as a new sorbent in future sample pretreatment technique.

Acknowledgements

Financial support from the Research Affairs of Shahid Beheshti University is gratefully acknowledged.

References

1. B. L. Wang, T. Takigawa, A. Takeuchi, Y. Yamasaki, H. Kataoka, D. H. Wang and K. Ogino *J. Occup. Health*, 2007, **49**, 104-110.

2. S. Suna, F. Jitsunari, F. Asakawa, T. Hirao, T. Mannami and T. Suzue, *J. Occup. Health*, 2005, **47**, 32874-32877.

3. I. Brcic and L. Skender, *J. Sep. Sci*., 2003, **26**, 1225-1229.

4. L. C. Holcomb and B. S. Seabrook, *Indoor Environ*., 1995, **4**, 7‑26.

5. Agency for Toxic Substances and Disease Registry (ATSDR), Atlanta, GA, 2007, pp. 438.

6. T. Schupp, H. M. Bolt, R. Jaeckh and J. G. Hengstler, *Toxicol. Lett*., 2006, **160**, 93–104.

7. I. Andersen, G. R. Lundqvist, L. Molhave, O. F. Pedersen, *Scand. J. Work Environ. Health*, 1983, **9**, 405–418.

8. Agency for Toxic Substances and Disease Registry (ATSDR), Atlanta, GA, 2000, pp. 357.

9. L. M. L. Nollet, Chromatographic analysis of the environment. CRC Press, 2006, New York, pp 513‑514.

10. C. Carrillo-Carrion, R. Lucena, S. Cardenas and M. Valcarcel, *J. Chromatogr. A,* 2007, **1171** 1–7.

11. M. A. Mottaleb, M. Z. Abedin and M. S. Islam, *Anal. Sci.*, 2003, **19**, 1365-1369. ·

12. A. Sarafraz-Yazdi, H. Piri moghadam, Z. Es'haghi and S. Sepehr, *Anal. Methods*., 2010, **2**, 746–752.

13. Z. Es'haghi, M. Ebrahimi and M. S. Hosseini*, J. Chromatogr. A*, 2011, **1218**, 3400-3406.

14. L. Xie, S. Liu, Z. Han, R. Jiang, H. Liu, F. Zhu, F. Zeng, C. Su and G. F. Ouyang, *Anal. Chim. Acta.*, 2015, **853**, 303-310.

15. M. B. Gholivand, M. Shamsipur, M. Shamizadeh, R. Moradian and B. Astinchap, *Anal. Chim. Acta.*, 2014, **822**, 30-36.

16. A. Sarafraz-Yazdi, S. H. Khaleghi-Miran and Z. Es'haghi, *Int. J. Environ. Anal. Chem.*, 2010, **90**, 1036–1047.

17. A. Sarafraz-Yazdi, A. H. Amiri and Z. Z. Es'haghi, *Talanta.*, 2009, **78**, 936–941.

18. V. Vickackaite and E. Pusvaskiene, *J. Sep. Sci.*, 2009, **32**, 3512–3520.

19. Y. Assadi, F. Ahmadi and M. R. Milani Hossieni, *Chromatographia.*, 2010, **71**, 1137–1141.

20. H. Faraji, A. Feizbakhsh and M. Helalizadeh, Microchim. Acta, 2013, **180**, 1141-1148.

21. A. Sarafraz-Yazdi, A. H. Amiri and Z. Es'haghi, *Chemosphere*, 2008, **71**, 671–676.

22. X. Ma, M. Huang, Z. Li and J. Wu, *J. Hazard. Mater.,* 2011, **194**, 24–29.

23. T. Shamspur and A. Mostafavi, *J. Hazard. Mater.,* 2009, **168**, 1548-1553.

24. S. Zhu, W. Niu, H. Li, S. Han and G. Xu, *Talanta.,* 2009, **79**, 1441-1445.

25. H. Tabani, K. Khodaei, Y. Bide, F. D. Zare, S. Mirzaei and A. R. Fakhari, *J. Chromatogr. A,* 2015, **1407**, 21–29.

26. J. M. Jimenez-Soto, S. Cardenas and M. Valcarcel, *J. Chromatogr. A*, 2009, **1216**, 5626-5633.

27. H. Tabani, A. R. Fakhari, A. Shahsavani, M. Behbahani, M. Salarian, A. Bagheri and S. Nojavan, *J. Chromatogr. A,* 2013, **1300**, 227– 235.

28. H. Zhang and H. K. Lee, *Anal. Chim. Acta.*, 2012, **742**, 67-73.

29. H. Zhang and H. K. Lee, *J. Chromatogr. A*, 2011, **1218**, 4509-4516.

30. H. Zhang, W. P. Low and H. K. Lee, *J. Chromatogr. A*, 2012, **1233**, 16-21.

31. C. Li and G. Q. Shi, *Nanoscale*, 2012, **4**, 5549-5563.

32. K. Gong, F. Du, Z. Xia, M. Duratock and L. Dai, *Science,* 2009, **323**, 760–764.

33. S. U. Lee, R. V. Belosludov, H. Mizuseki and Y. Kawazoe, *Small*, 2009, **5**, 1769–1775.

34. S. Hu, A. Wang, X. Li and H. Lowe, *J. Phys. Chem. Solids*, 2010, **71**, 156-162.

35. S. K. Movahed, M. Dabiri and A. Bazgir, *Appl. Catal. A,* 2014, **488,** 265–274.

36. D. Long, W. Li, L. Ling, J. Miyawaki, I. Mochida and S.H. Yoon, *Langmuir*, 2010, **26**, 16096-16102.

37. L. Sun, L. Wang, C. Tian, T. Tan, Y. Xie, K. Shi, M. Li and H. Fu, *RSC Adv.,* 2012, **2**, 4498-4506.

38. X. Zhu, P. Zhang, S. Xu, X. Yan and Q. Xue, *ACS Appl. Mater. Interfaces,* 2014, **6**, 11665-11674.

39. A. R. Fakhari, H. Tabani, S. Nojavan and H. Abedi, *Electrophoresis,* 2012, **33**, 506–515.

40. A. Jorio, M. S. Dresselhaus, R. Saito and G. F. Dresselhaus, Wiley-VCH: Berlin, 2011.

41. X. Fu, F. Bei, X. Wang and S. O'Brien, *Lombardi J. R. Nanoscale.*, 2010, **2**, 1461-1466.

42. D. Deng, X. Pan, L. Yu, Y. Cui, Y. Jiang, J. Qi, W. X. Li, Q. Fu, X. Ma, Q. Xue, G. Sun and X. Bao, *Chem. Mater*., 2011, **23**, 1188-1193.

43. Z. Y. Yang, Y. X. Zhang, L. Jing, Y. F. Zhao, Y. M. Yan and K. N. Sun, *J. Mater. Chem. A*, 2014, **2**, 2623-2627.

44. H. Hu, Z. Zhao, W. Wan, Y. Gogotsi and *J.* Qiu, *Adv. Mater*., 2013, **25**, 2219-2223.

45. J. Wang, Z. Shi, J. Fan, Y. Ge, J. Yin and G. Hu, *J. Mater. Chem.,* 2012, **22**, 22459-22466.

46. P. Wu, Y. Qian, P. Du, H. Zhang and C. Cai, *J. Mater. Chem*., 2012, **22**, 6402-6412.

47. H. Tabani, A. R. Fakhari and A. Shahsavani, *Electrophoresis,* 2013, **34**, 269–276.

48. A. R. Fakhari, H. Tabani and S. Nojavan, *Drug Test. Analysis,* 2013, **5**, 589–595.

49. L. Nouri, I. Ghodbane, O. Hamdaoui, and M. Chiha, *J. Hazard. Mater.,* 2007, **149**, 115–125.

50. S. S. Baral, S. N. Das, and P. Rath, *Biochem. Engin. J.*, 2006, **31**, 216– 222,.

51. W. Zheng, X. Li, F. Wang, Q. Yang, P. Deng, and G. Zeng, *J. Hazard. Mater*., 2008, **157**, 490–495.

52. M. Havelcova, J. Mizera, I. Skorova, and M. Pekar, *J. Hazard. Mater.,* 2009, **161**, 559–564.

53. Z. Shahryari, A. S. Goharrizi, and M. Azadi, Int. *J. Water Resour. Environ. Eng.,* 2010, **2**, 16–28.

Figure captions

Fig. 1. Raman spectra of GO, ND-G, HND-G and 3D-HND-G.

Fig 2. Graphical structure of ND-G, HND-G and 3D-HND-G.

Fig. 3. TEM images of a) ND-G, b) HND-G and c) 3D-HNG-G; SEM image of 3D-HND-G.

Fig. 4. XRD patterns of GO, NG, HNG and 3D-HNG.

Fig. 5 FT-IR spectra of GO, NG, HNG and 3D-HNG.

Fig. 6. Full-range XPS spectra of NG, HNG and 3D-HNG composites and related N 1s core-level region

Fig. 7. Effect of the sorbent type on the adsorption efficiency of BTEX compounds. (Extraction conditions: sample solution, 100 mL of 100 ng mL^{-1} of each analyte; amount of adsorbent, 50 mg; sorption time, 10 min; 500 µL methanol as eluent solvent, and without addition of NaCl).

Fig. 8. Effect of the pH of the sample on the adsorption efficiency of BTEX compounds. (Extraction conditions: sample solution, 100 mL of 100 ng mL^{-1} of each analyte; amount of adsorbent, 50 mg; sorption time, 10 min; 500 µL methanol as eluent solvent, and without addition of NaCl).

Fig. 9. Pareto chart of the main effects in the BBD.

Fig. 10. RSM and contour plots obtained by plotting of **A)** amount of sorbent vs. the extraction time, and **B)** Salt content vs. volume of eluent using the BBD.

Fig. 11. Langmuir isotherms applied to adsorption of BTEX by 3D-HND-G.

Fig. 12. Freundlich isotherms applied to adsorption of BTEX by 3D-HND-G.

Fig. 13. Chromatograms obtained after SPE from **A)** non-spiked Talab Bande Alikhani river sample, **B)** Talab Bande Alikhani river sample spiked at a concentration level of 60 ng mL^{-1} of each BTEX, **C)** non-spiked Farahzad river sample, **D)** Farahzad river sample spiked at a concentration level of 60 ng mL^{-1} of each BTEX. (Extraction condition: 100 mL sample

solution; 255 μL methanol as eluent solvent; 70 mg amount of 3D-HND-G as sorbent; extraction time: 8 min; and 6.5% (w/v) NaCl; 1: Benzene, 2: Toluene, 3: Ethyl Benzene, 4: Xylene).

Table 1 The nitrogen, carbon, hydrogen content of ND-G, HND-G and 3D-HND-G.

Entry	N content%	C content%	H content%	N/C
ND-G	3.19	70.25	1.39	0.04
HND-G	11.24	65.81	2.03	0.17
3D-HND-G	17.44	52.80	4.39	0.33

Table 2 The experimental variables and levels of the BBD.

Variable	key	Level		
		Lower	Central	Upper
Extraction time (min)	A	2	7	12
Amount of sorbent (mg)	B	10	55	100
Salt content (% w/v)	C	0	5	10
Volume of eluent (μL)	D	100	300	500

Table 3 Results of ANOVA for the fitted model.

Source	Sum of Squares	Df	Mean Square	F-Ratio	P-Value
A	8472.9	1	8472.9	2.58	0.1690
B	56492.1	1	56492.1	17.21	0.0089
C	152986.0	1	152986.0	46.61	0.0010
D	9047.07	1	9047.07	2.76	0.1578
AA	303156.0	1	303156.0	92.37	0.0002
AB	1228.5	1	1228.5	0.37	0.5674
AC	438.902	1	438.902	0.13	0.7296
AD	778.41	1	778.41	0.24	0.6469
BB	448249.0	1	448249.0	136.57	0.0001
BC	1768.2	1	1768.2	0.54	0.4959
BD	1228.5	1	1228.5	0.37	0.5674
CC	219096.0	1	219096.0	66.75	0.0004
CD	264.403	1	264.403	0.14	0.722
DD	27387.2	1	27387.2	8.34	0.0343
Lack-of-fit	11458.0	10	1145.8	0.35	0.9263
Pure error	16410.6	5	3282.12		

Table 4 Isotherm parameters for adsorption of BTEX compounds onto 3D-HND-G.

Analytes	Langmuir			Freundlich		
	Q_m (mg g^{-1})	K_l (L. mg^{-1})	R^2	n	K_f (mg g^{-1})(L. mg^{-1})$^{1/n}$	R^2
Benzene	130	0.008	0.9099	1.23	1.606	0.9879
Toluene	103	0.01	0.8704	1.26	1.547	0.9962
Ethyl benzene	92	0.011	0.8741	1.29	1.580	0.9946
o-Xylene	88	0.012	0.9169	1.29	1.560	0.9961

Table 5 Figures of merit of proposed method for determination of BTEX compounds from aqueous samples.

[a] Concentration is based on ng mL^{-1}.

Analytes	r	LOD[a]	LOQ[a]	Linearity[a]	EF	Recovery%[b]	RSD%[c]	
							Intra day	Inter day
Benzene	0.9985	0.5	1.5	1.5-500	376	94	5.0	4.5
Toluene	0.9978	1.0	3.0	3.0-500	348	87	4.4	5.2
Ethyl benzene	0.9968	1.0	3.0	3.0-500	328	82	4.5	4.9
o-Xylene	0.9977	1.0	3.0	3.0-500	328	82	4.2	4.8

[b] Recovery was obtained for 60 ng mL^{-1} of herbicide (n = 5).

[c] Intra day and inter day RSDs% were obtained by five replicate measurements for 60 ng mL^{-1} of each BTEX compound.

Table 6. Determination of the target compounds in the certified reference materials.

Analytes	CRM 1				CRM 2			
	Calculated concentration[a] (ng mL^{-1})	*Found concentration* (ng mL^{-1})	*RR%*	RSD%	*Calculated concentration*[a] (ng mL^{-1})	*Found concentration* (ng mL^{-1})	*RR%*	*RSD%*
Benzene	30	29.5	98.3	5.5	100	100	100	4.1
Toluene	30	31	103.3	4.9	100	99	99	3.9
Ethyl benzene	30	30.5	101.6	4.8	100	99.5	99.5	4.2
o-Xylene	30	31	103.3	5.4	100	100.5	100.5	4.0

[a] The calculation is based on the certified reference value and the final dilution of the sample.

Table 7 Determination of BTEX compounds in river water samples.

River Water [a]		Benzene	Toluene	Ethyl benzene	o-Xylene
RW 1	Initial concentration (ng mL^{-1})	n.d[c]	n.d[c]	n.d[c]	n.d[c]
	RR%[b]	102	104	98	102
	RSD% (n=4)	4.9	5.1	5.2	5.0
RW 2	Initial concentration (ng mL^{-1})	n.d[c]	n.d[c]	n.d[c]	n.d[c]
	RR%[b]	95	93	94	98
	RSD% (n=4)	5.5	5.9	5.8	5.4
RW 3	Initial concentration (ng mL^{-1})	24	32	n.d[c]	n.d[c]
	RR%[b]	104	101	99	98
	RSD% (n=4)	3.7	3.3	3.4	3.9
RW 4	Initial concentration (ng mL^{-1})	68	45	n.d[c]	n.d[c]
	RR%[b]	97	96	94	94
	RSD% (n=4)	5.4	5.6	6.2	6.0
RW 5	Initial concentration (ng mL^{-1})	n.d[c]	n.d[c]	n.d[c]	n.d[c]
	RR%[b]	100	99	96	95
	RSD% (n=4)	5.0	4.3	4.2	4.9

[a] RW 1: Kan, RW 2: Jajrood, RW 3: Farahzad, RW 4: Talab Bande Alikhani, RW 5: Mohammadieh.

[b] 60 ng mL^{-1} of each drug was added to calculate relative recovery percent (RR%).

[c] n.d, not detected.

Table 8 Comparison of analytical performance data of proposed method with other methods applied for the quantification of BTEX compounds.

Method	Sample preparation	LOD[a]	EF	RR%	RSD%	Ref.
GC-MS	LLE	0.26-0.72	-	-	2.5-5.0	10
GC-FID	SPE	104-372	-	76-87	2.9-3.5	11
GC-FID	SPME	0.01-10	628-733	106-113	2.3-4.0	12
GC-FID	SDME	5.0-10	43.8-64.5	85.5-91.2	4.7-7.7	17
GC-MS	SDME	0.02-0.09	-	88.9-103.1	3.0-5.2	16
GC-FID	DLLME	0.1-0.2	122-311	76.0-101	0.9-6.4	19
GC-FID	DLLME	0.1-0.35	87-290	94,6-105.9	8-12	18
GC-FID	Modified DLLME	0.04-0.09	301-514	85.6-102.4	2.1-4.1	20
GC-FID	HF-LPME	4.8-30	41.5-128	89-92	2.0-4.6	21
GC-FID	HF-LPME	2.2-4.0	-	90-111.5	1.3-3.5	22
GC-FID	Modified SPE	0.5-1.0	328-376	93-104	4.4-5.2	Proposed method

[a] All concentrations are based on ng mL^{-1}.

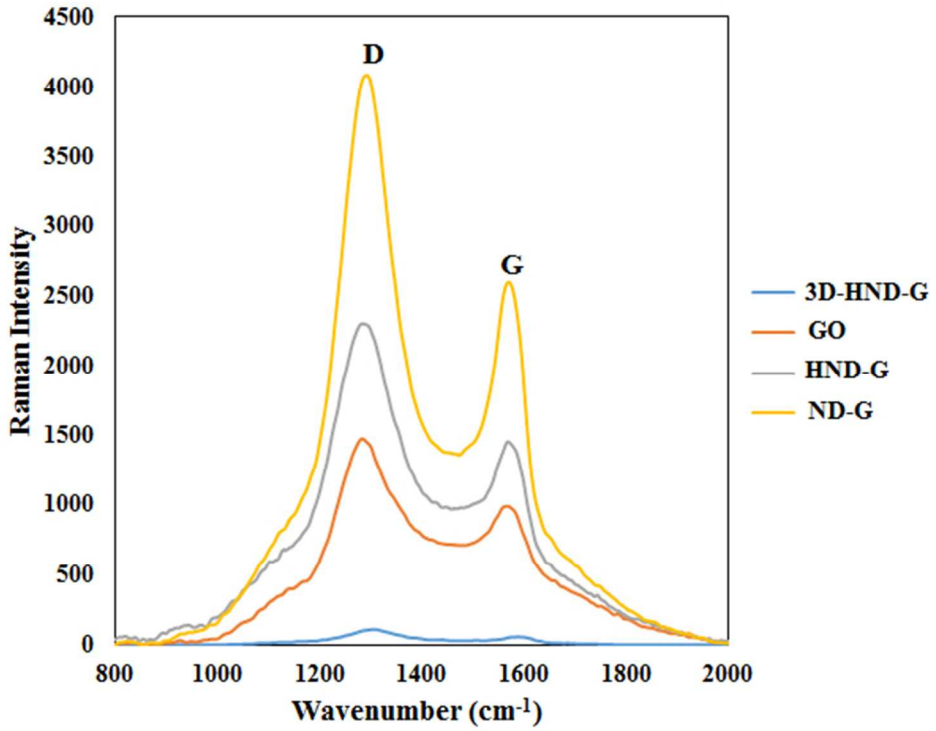

167x128mm (96 x 96 DPI)

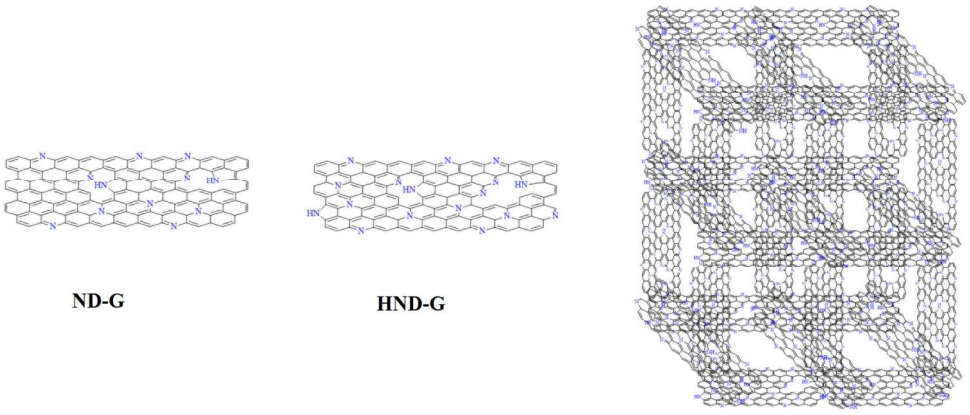

152x66mm (300 x 300 DPI)

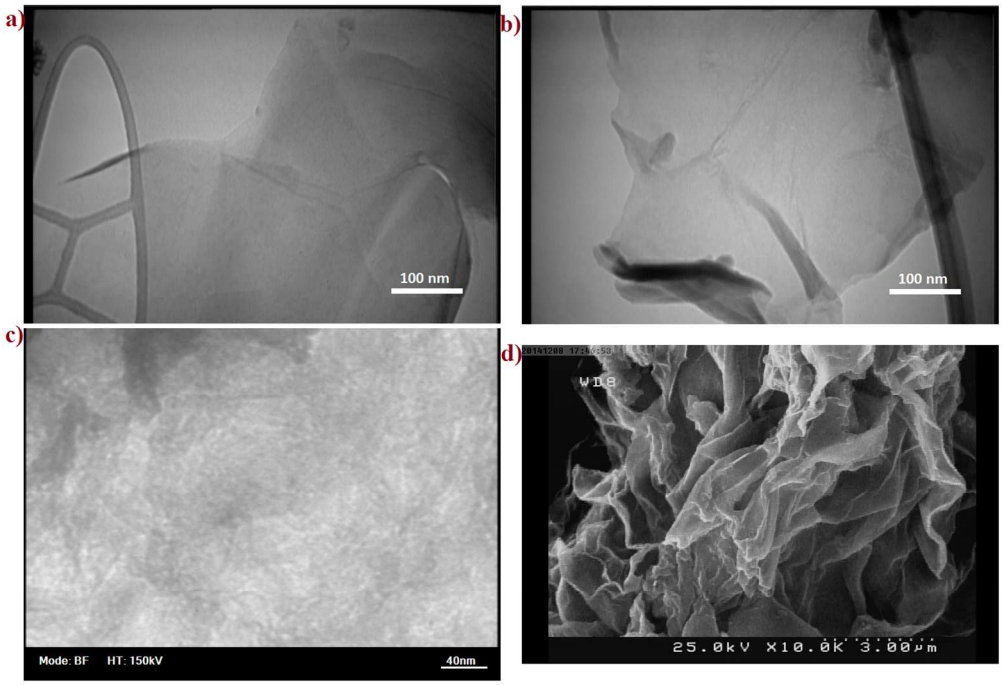

127x87mm (300 x 300 DPI)

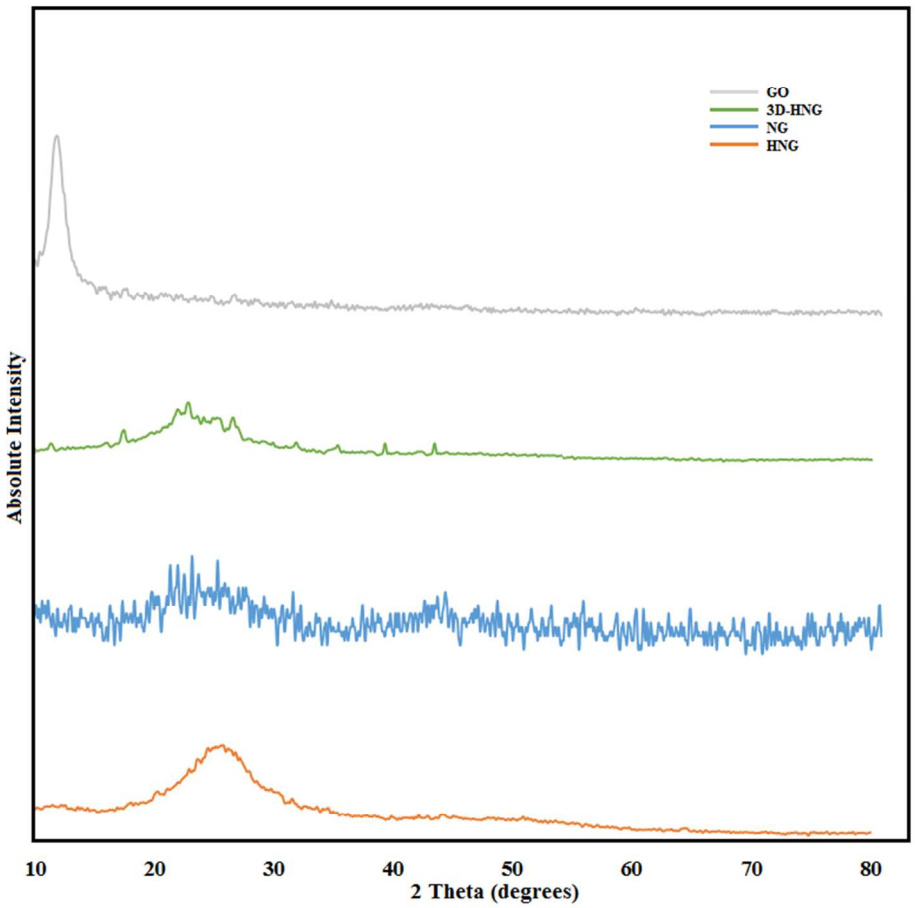

224x208mm (96 x 96 DPI)

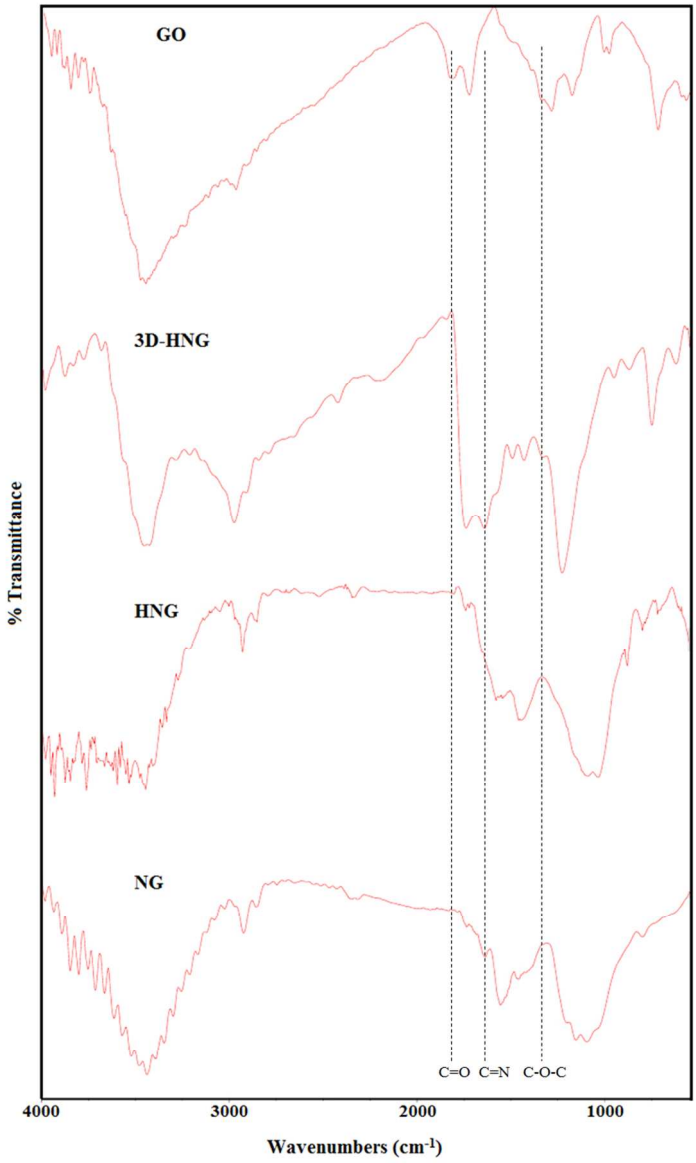

236x379mm (96 x 96 DPI)

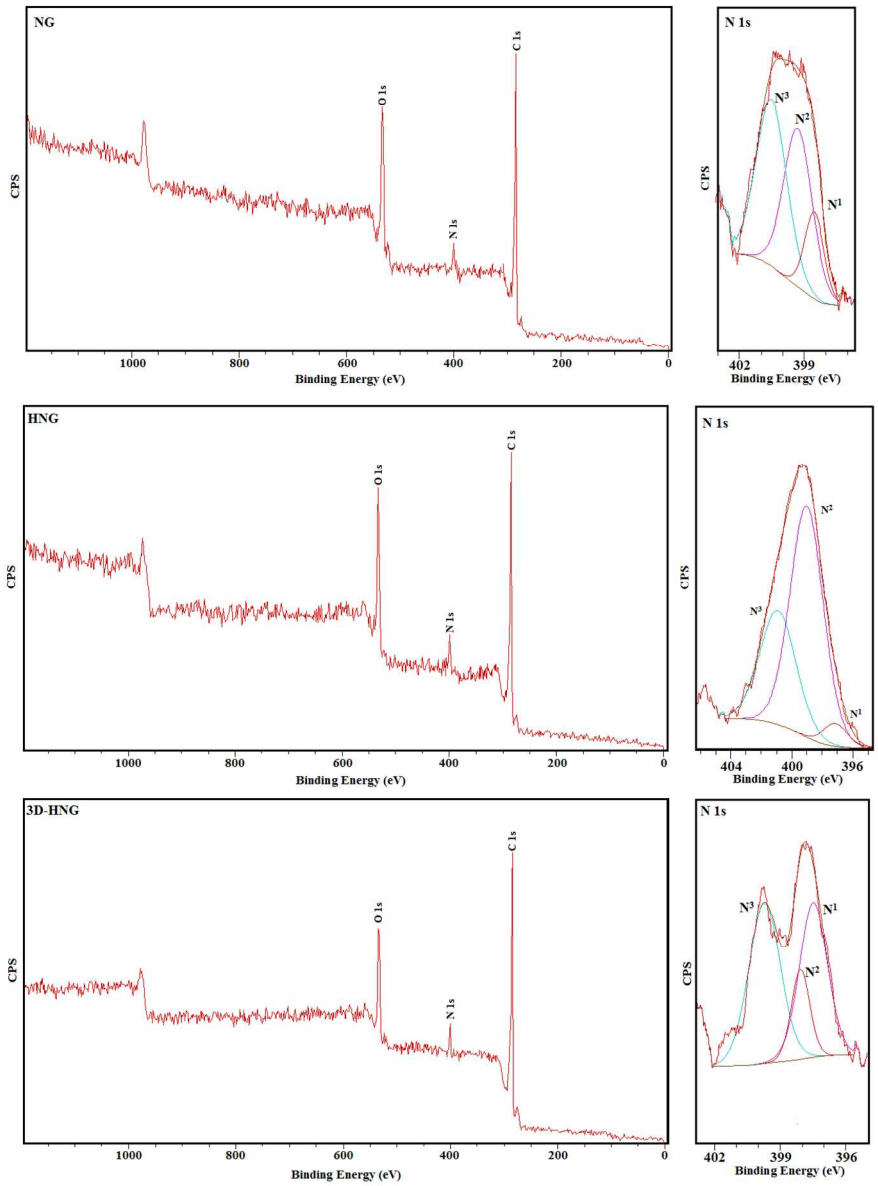

352x479mm (96 x 96 DPI)

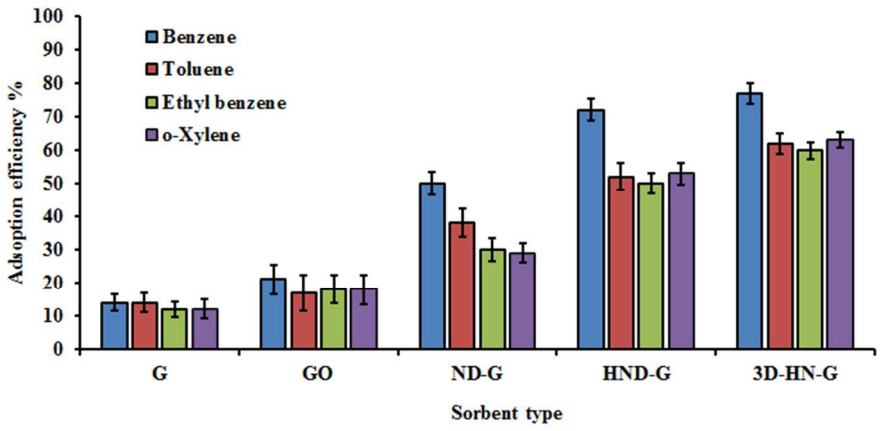

206x100mm (96 x 96 DPI)

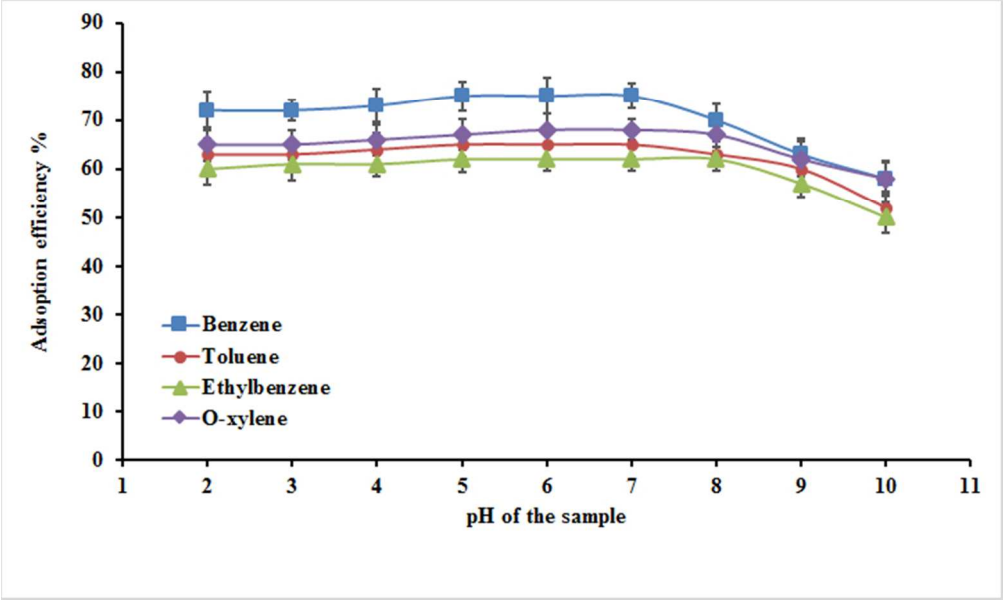

191x114mm (96 x 96 DPI)

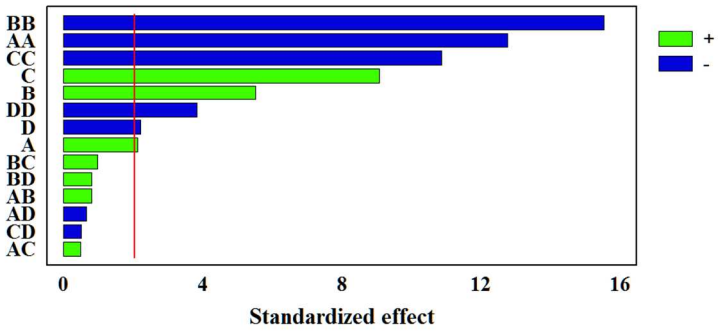

228x100mm (150 x 150 DPI)

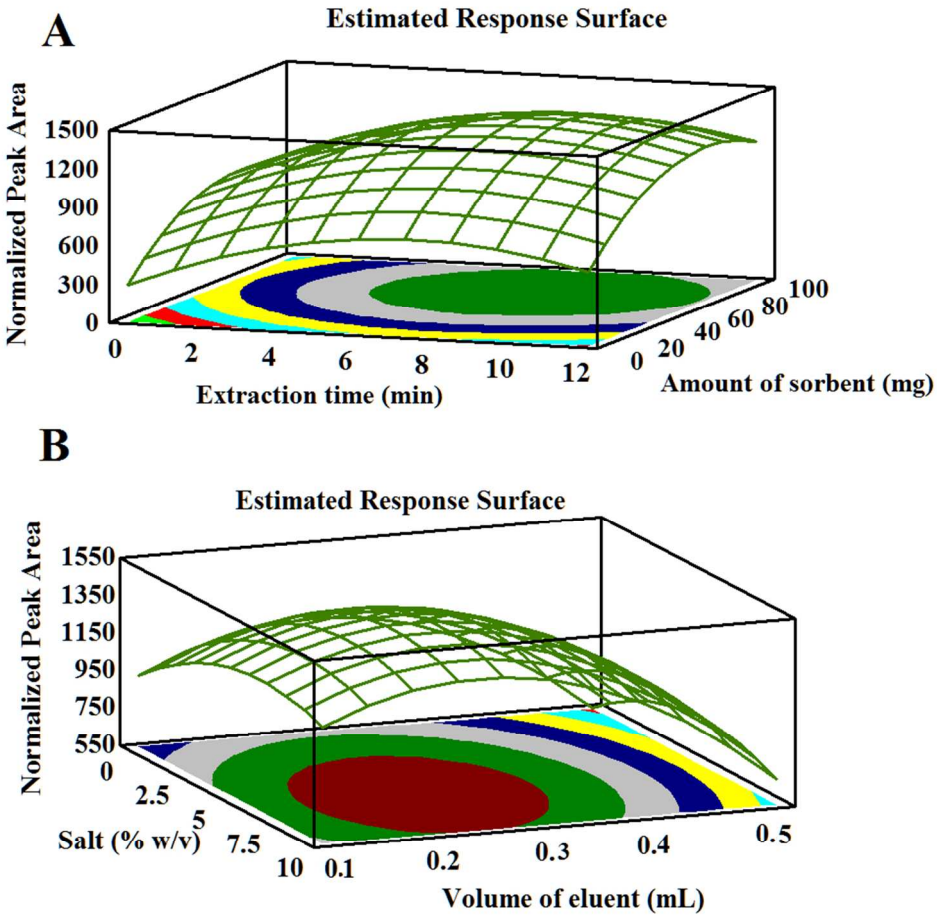

270x259mm (96 x 96 DPI)

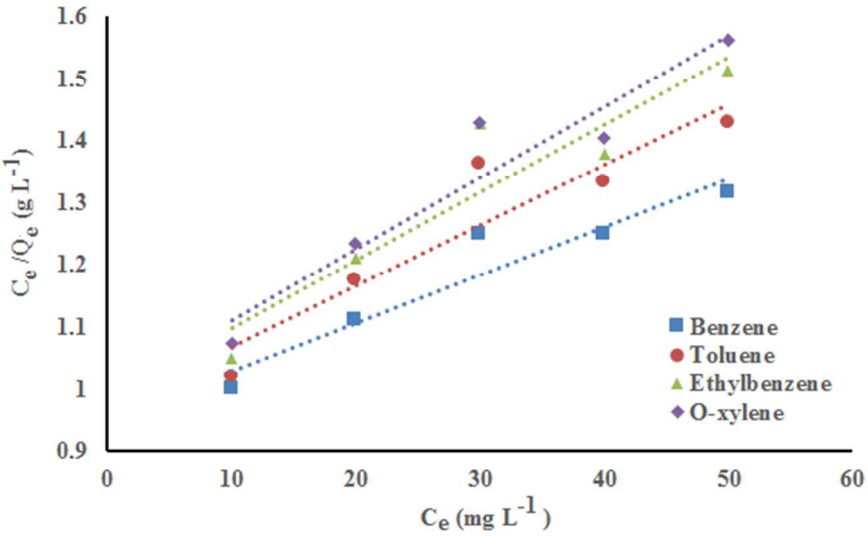

172x101mm (96 x 96 DPI)

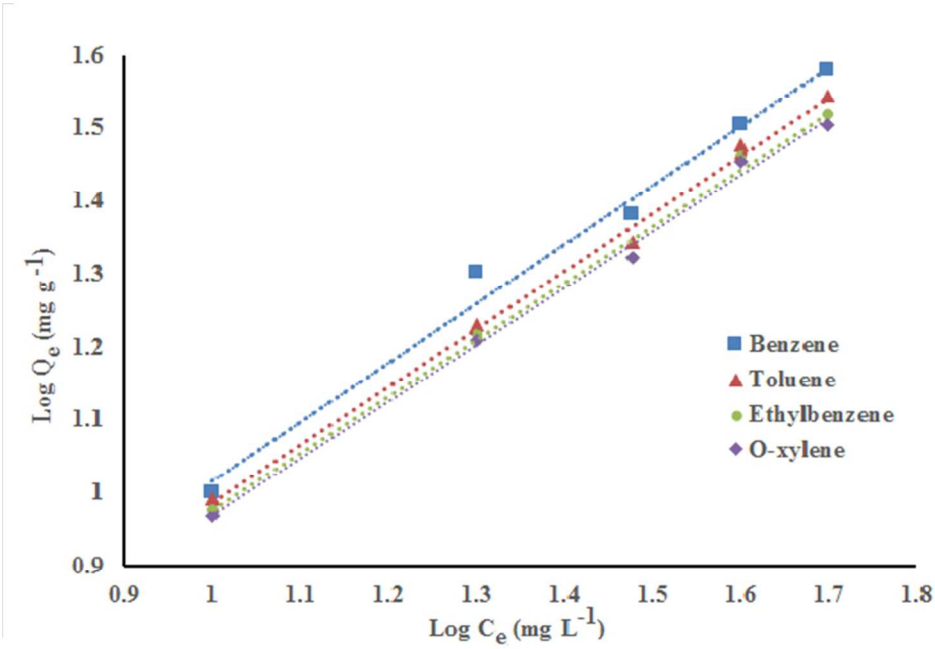

173x114mm (96 x 96 DPI)

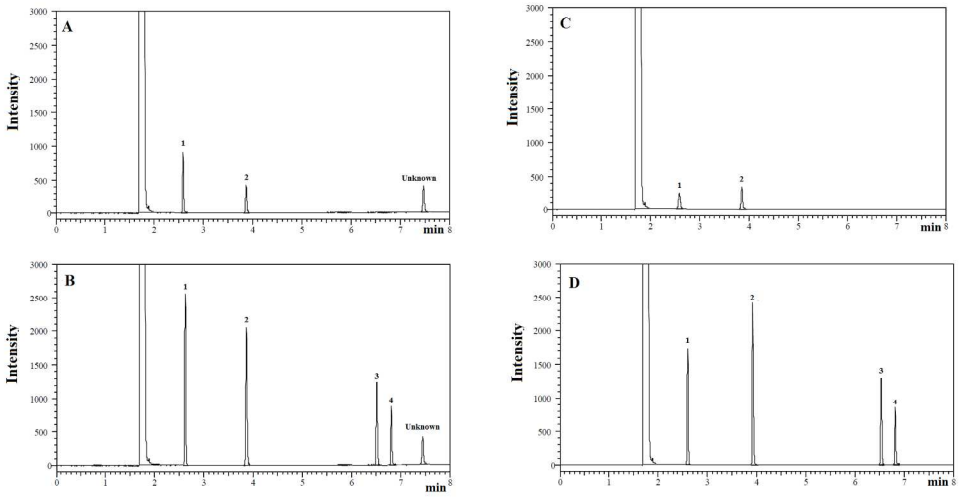

597x306mm (96 x 96 DPI)

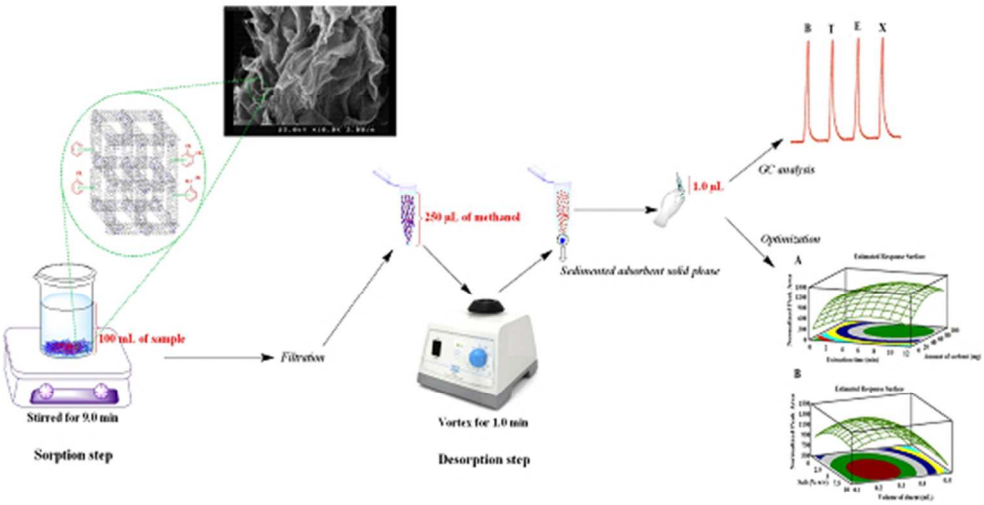

A simple and highly sensitive method that involves SPE–GC with three dimensional high nitrogen doped graphene as a novel sorbent used for determination of BTEX compounds in environmental samples.

153x106mm (96 x 96 DPI)